PHYSICAL REVIEW B VOLUME 43, NUMBER 3 15 JANUARY 1991-II

Efficient pseudopotentials for plane-wave calculations

N. Troullier and José Luís Martins
Department of Chemical Engineering and Materials Science, University of Minnesota, Minneapolis, Minnesota 55455
(Received 3 August 1990)

We present a simple procedure to generate first-principles norm-conserving pseudopotentials, which are designed to be smooth and therefore save computational resources when used with a plane-wave basis. We found that these pseudopotentials are extremely efficient for the cases where the plane-wave expansion has a slow convergence, in particular, for systems containing first-row elements, transition metals, and rare-earth elements. The wide applicability of the pseudopotentials are exemplified with plane-wave calculations for copper, zinc blende, diamond, α-quartz, rutile, and cerium.

I. INTRODUCTION

Electronic-structure calculations performed within the framework of the local-density approximation (LDA) (Ref. 1) have demonstrated their ability to accurately predict different physical properties. Even with major advances in computer technology, the magnitude of the computational effort needed to calculate the physical properties of complex crystals is still enormous, and therefore a large interest exists for improving the computational methods for the electronic structure of solids.

Replacing the effect that the chemically inert core states exert on the chemically active valence states by an effective pseudopotential, dates back to the early work of Fermi[2] and has seen a sizeable amount of interest and further developments since the seminal work of Phillips and Kleinman.[3] The physically reasoning behind the pseudopotential approximation is simple: since the core-electron wave functions of an atom remain essentially unchanged when placed into different chemical environments and since that the core wave functions' only major contribution to chemical bonding is to enforce the valence wave functions orthogonality to the core states, the true atomic potential can justifiably be replaced by a pseudopotential that effectively reproduces the effects of the core electrons. With only this physical constraint, an infinite number of pseudopotentials can be generated and it has been the objective of much active work to try to determine what auxiliary conditions are needed to produce a pseudopotential that both adequately reproduces the all-electron behavior outside the core region when placed in different chemical environments, and is still computational efficient.

Mathematically and numerically, a plane-wave-basis formalism[4] is one of the simplest and most natural formalism to implement for crystals. However, expanding the core wave functions or the core oscillatory region of the valence wave functions into plane waves is extremely inefficient. Therefore, plane-wave basis sets are practically always used in conjunction with the pseudopotential approximation. This combination of pseudopotentials and plane waves has become one of the most popular methods for electronic structure calculations.[5] Traditionally the pseudopotential plane-wave method has been considered impractical for systems containing transition and rare-earth metals, and inefficient for the most electronegative first-row elements. To handle crystal systems containing these elements, other basis sets such as Gaussians, linearized-augmented plane waves (LAPW), linear muffin-tin orbitals (LMTO), and mixed basis sets[6] are commonly used. With the development of diagonalization methods that can handle a basis set of several thousand plane waves,[7] there is no compelling reason why these former impossibilities cannot be studied with the pseudopotential plane-wave method. The examples discussed in Sec. V of this paper will amply demonstrate that the pseudopotential plane-wave method can be efficiently used in LDA calculations for any type of material, including transition metals and rare earths.

In this paper we present a pseudopotential-generation method which produces computationally efficient pseudopotentials for use with a plane-wave basis set, particularly for first-row, transition metal and rare-earth elements. In Sec. II we present a brief review of the pseudopotential method, followed by the problem of generating smooth pseudopotentials in Sec. III. A simple recipe for soft pseudopotentials is presented in Sec. IV, which is substantial improved over an earlier version previously discussed in a short communication.[8] Finally, in Sec. V the properties of these pseudopotentials are exemplified with calculations for copper, zinc blende, diamond, α-quartz, rutile, and cerium. Atomic units are used throughout this paper unless otherwise indicated.

II. GENERAL PSEUDOPOTENTIAL THEORY

The majority of the pseudopotentials currently used in electronic-structure calculations are generated from all-electron atomic calculations. Within the density-functional theory this is done by assuming a spherical screening approximation and self-consistently solving the radial Kohn-Sham equation[1]

$$\left[\frac{-1}{2}\frac{d^2}{dr^2}+\frac{l(l+1)}{2r^2}+V[\rho;r]\right]rR_{nl}(r)=\varepsilon_{nl}rR_{nl}(r)\ , \tag{1}$$

where $V[\rho;r]$ is the self-consistent one-electron potential

$$V[\rho;r]=\frac{-Z}{r}+V_{\rm H}[\rho;r]+V_{\rm xc}^{\rm LDA}(\rho(r)) , \quad (2)$$

$\rho(r)$ is the sum of the electron densities for the occupied wave functions $R_{nl}(r)$, $V_{\rm H}[\rho;r]$ is the Hartree potential, and $V_{\rm xc}^{\rm LDA}(\rho(r))$ is the local-density approximation for the exchange-correlation potential. Most pseudopotentials are then constructed such that they satisfy four general conditions.[9–13] The first is that the valence (the principal quantum number n is further omitted for simplicity) pseudo-wave-functions generated from the pseudopotential should contain no nodes. This stems from the fact that we would like to construct smooth pseudo-wave-functions and therefore the wiggles associated with the nodes are undesirable. Second, the normalized atomic radial pseudo-wave-function (PP) with angular momentum l is equal to the normalized radial all-electron wave function (AE) beyond a chosen cutoff[10] radius r_{cl},

$$R_l^{\rm PP}(r)=R_l^{\rm AE}(r) \quad \text{for } r>r_{cl} , \quad (3)$$

or converges rapidly to that value.[9,11–13] Third, the charge enclosed within r_{cl} for the two wave functions must be equal,[9]

$$\int_0^{r_{cl}}|R_l^{\rm PP}(r)|^2r^2\,dr=\int_0^{r_{cl}}|R_l^{\rm AE}(r)|^2r^2\,dr . \quad (4)$$

Last, almost redundantly, the valence all-electron and pseudopotential eigenvalues must be equal,

$$\varepsilon_l^{\rm PP}=\varepsilon_l^{\rm AE} . \quad (5)$$

If a pseudopotential meets the conditions outlined above, it is commonly referred to as a "norm-conserving pseudopotential."[9] Constructing a pseudo-wave-function that fulfills these requirements can be accomplished using many different schemes.[8–13] The nonuniqueness of these pseudopotentials is a clear indication of the available variational freedom that we will exploit to produce a smooth pseudopotential. Once the pseudo-wave-function is obtained, the screened (scr) pseudopotential is then recovered by inversion of the radial Schrödinger equation [Eq. (1)],

$$V_{{\rm scr},l}^{\rm PP}(r)=\varepsilon_l-\frac{l(l+1)}{2r^2}+\frac{1}{2rR_l^{\rm PP}(r)}\frac{d^2}{dr^2}[rR_l^{\rm PP}(r)] . \quad (6)$$

According to Eq. (6), for a nodeless pseudo-wave-function the pseudopotential does not have any singularities, except possibly at the origin. From Eq. (6) we can also see two more important details, if we wish the pseudopotential to be continuous, then the pseudo-wave-function must have continuous derivatives up to and including the second derivative, and that if we wish to avoid a hard-core pseudopotential with a singularity at the origin, the pseudo-wave-function must behave as r^l near the origin.

The screening from the valence electrons depends strongly on the environment in which they are placed. If we remove the screening effects of the valence electrons and generate an ionic pseudopotential, we can then use this potential in a self-consistent procedure to determine the electron screening in other environments. This is done by subtracting the Hartree $V_{\rm H}^{\rm PP}(r)$ and exchange-correlation $V_{\rm xc}^{\rm PP}(r)$ potentials calculated from the valence pseudo-wave-functions from the screened potential to generate an ionic pseudopotential,

$$V_{{\rm ion},l}^{\rm PP}(r)=V_{{\rm scr},l}^{\rm PP}(r)-V_{\rm H}^{\rm PP}(r)-V_{\rm xc}^{\rm PP}(r) . \quad (7)$$

A major consequence of the pseudopotential generation procedure just outlined is that each angular-momentum component of the wave function will see a different potential. The ionic pseudopotential operator is then,

$$\hat{V}_{\rm ion}^{\rm PP}(r)=V_{\rm ion,local}^{\rm PP}(r)+\sum_l V_{{\rm nonlocal},l}(r)\hat{P}_l , \quad (8)$$

where $V_{\rm ion,local}^{\rm PP}(r)$ is the local potential and,

$$V_{{\rm nonlocal},l}(r)=V_{{\rm ion},l}^{\rm PP}(r)-V_{\rm ion,local}^{\rm PP}(r) \quad (9)$$

is the nonlocal (or more precisely semilocal) potential for the angular-momentum component l, and $\hat{P}_l$ projects out the lth angular-momentum component from the wave function. The local potential can, in principle, be arbitrarily chosen, but since the summation in Eq. (8) will need to be truncated at some value of l, the local potential should be chosen such that it adequately reproduces the atomic scattering for all the higher angular-momentum channels.

The semilocal potential [Eq. (9)] can be transformed into a nonlocal form by using a procedure suggested by Kleinman and Bylander (KB),[14]

$$V_{{\rm nonlocal},l}^{\rm KB}(r)=\frac{|V_{{\rm nonlocal},l}(r)\Phi_l^{{\rm PP},0}(r)\rangle\langle\Phi_l^{{\rm PP},0}(r)V_{{\rm nonlocal},l}(r)|}{\langle\Phi_l^{{\rm PP},0}(r)|V_{{\rm nonlocal},l}(r)|\Phi_l^{{\rm PP},0}(r)\rangle} , \quad (10)$$

where $V_{{\rm nonlocal},l}(r)$ is the semilocal potential [Eq. (9)], and $\Phi_l^{{\rm PP},0}(r)$ is the atomic reference pseudo-wave-function, including the angular-momentum component for which the pseudopotential was calculated. Substantial savings in computer time and storage can be achieved using this separable nonlocal expression.

Hidden in Eqs. (3) and (5) is an important detail that we should further elaborate upon. The radial Schrödinger equation is a second-order linear differential equation. Given the screened all-electron potential and an energy ε (not necessarily an eigenvalue), the solution of the equation is uniquely defined by the value of the wave function $R(r)$ and its derivative $R'(r)$ at any given point r_0. Neglecting normalization, the wave function is then uniquely determined by its logarithmic derivative

$$\frac{d}{dr}\ln[R_l(r,\varepsilon)]\bigg|_{r=r_0}=\frac{1}{R_l(r,\varepsilon)}\frac{dR_l(r,\varepsilon)}{dr}\bigg|_{r=r_0} \quad (11)$$

at the point r_0. If the screened all-electron potentials and pseudopotentials are identical outside the radius r_{cl}, then the all-electron wave-function and pseudo-wave-functions are proportional outside r_{cl} if

$$\frac{1}{R_l^{\mathrm{PP}}(r,\varepsilon)}\frac{dR_l^{\mathrm{PP}}(r,\varepsilon)}{dr}=\frac{1}{R_l^{\mathrm{AE}}(r,\varepsilon)}\frac{dR_l^{\mathrm{AE}}(r,\varepsilon)}{dr} . \quad (12)$$

By construction this is true for a pseudopotential obeying Eqs. (3) to (5) for the eigenvalue energy ε_l. For a "perfect" pseudopotential, this equality would hold for all energies close to ε_l and above the core-state energies. The norm-conservation condition [Eq. (4)] imposes that the above equality is closely satisfied for a region surrounding ε_l, this follows because the solutions of the radial Schrödinger equation obey a version of the Friedel sum rule[9,15]

$$-\frac{1}{2}\frac{\partial}{\partial\varepsilon}\frac{\partial}{\partial r}\ln R(r,\varepsilon)\Big|_{\substack{\varepsilon=\varepsilon_l\\ r=r_{cl}}}=\frac{1}{r_{cl}^2R^2(r_{cl},\varepsilon_l)}\int_0^{r_{cl}}R^2(r,\varepsilon_l)r^2dr . \quad (13)$$

Comparing the logarithmic derivatives [Eq. (12)] of the all-electron and the pseudopotential wave functions as a function of the energy ε, at a radius $r_0\geq r_{cl}$, for the range of energies of the valence and lower conduction bands in the solid provides a quick picture of the quality of the pseudopotential. Often r_0 is taken as the Wigner-Seitz radius, but any useful radii can be used. However, the logarithmic derivatives are calculated assuming that the electron screening part of the potential is a constant. This is not the case when the atomic environment changes, and therefore a logarithmic derivative comparison should not be taken as an absolute test of the quality of an ionic pseudopotential.

The pseudopotential will accurately reproduce the all-electron calculation in the reference configuration in which it was generated. In practice we want it to closely reproduce other all-electron calculations in different environments, that is we want it to be "transferable." The logarithmic derivatives provide a first test of the transferability of the screened pseudopotential. Comparing the all-electron calculations for excited atomic states provides an easy way to test the ionic pseudopotential. Doing the same comparison for a prototypical crystal is, of course, a better test of the transferability of the pseudopotential, but it is also a more elaborate costlier test.

A possible method to improve the transferability to the solid is to generate the pseudopotential using an atomic configuration that as closely as possible mimics the environment in which it will be placed. This may require the use of nonbound or noneigenvalued wave functions, as recently suggested by Hamann.[16] In general, ionic pseudopotentials are insensitive to reasonable variations in the reference atomic configuration (or otherwise they would not be transferable) and the improvements obtained in this fashion are limited. Shirley *et al.*[17] proposed equating additional energy derivatives of the logarithmic derivatives of the wave function [Eq. (12)], that is generalizing Eq. (13), but have found that the corrections achieved by setting the second energy derivative were small and not comparable to the other errors present within the local-density approximation. The easiest approach to increase the pseudopotential tranferability is to simply decrease the cutoff radius r_{cl} used to generate the pseudopotential and pseudo-wave-functions, thereby reducing the difference between the all-electron and pseudopotential results. However, there are practical limits on how far we can decrease r_{cl} for example r_{cl} must be larger than the outermost node of the all-electron wave function if we insist on having nodeless pseudo-wave-functions.

III. PSEUDOPOTENTIAL SMOOTHNESS

A "smooth" pseudopotential is one in which there is a rapid convergence in the calculated total energy of a system, and therefore a rapid convergence of the systems properties, with respect to an increase in the plane-wave basis set. This convergence must be obtained irrespective of the particular choice of the representative crystal structure, its lattice constant, or any internal atomic positions. The Schrödinger equation for a crystal using a plane-wave basis set and the pseudopotential approximation is written as[4,5]

$$\sum_j H_{ij}(\mathbf{k})a(\mathbf{G}_j+\mathbf{k})=\varepsilon a(\mathbf{G}_i+\mathbf{k}) , \quad (14)$$

where $H_{ij}(\mathbf{k})$ is the momentum-space Hamiltonian matrix for point $\mathbf{k}$ in the Brillouin zone,

$$H_{ij}(\mathbf{k})=\tfrac{1}{2}\delta_{ij}|\mathbf{G}_i+\mathbf{k}|^2+V_{\mathrm{local}}(\mathbf{G}_i-\mathbf{G}_j)+\sum_l V_{\mathrm{nonlocal},l}(\mathbf{G}_i+\mathbf{k},\mathbf{G}_j+\mathbf{k}) , \quad (15)$$

the first term is the diagonal kinetic-energy operator, $V_{\mathrm{local}}(\mathbf{q})$ is the Fourier-transformed local potential $V_{\mathrm{local}}(r)$, which includes the self-consistent electron screening potential, $V_{\mathrm{nonlocal},l}(\mathbf{q},\mathbf{q}')$ is the momentum space representation of the nonlocal potential $V_{\mathrm{nonlocal},l}(r)$, and the $a(\mathbf{G}_j+\mathbf{k})$'s are the coefficients of the plane-wave expansion (Fourier series) of the wave function,

$$\Psi_{\mathbf{k}}(\mathbf{r})=\sum_j a(\mathbf{G}_j+\mathbf{k})e^{i(\mathbf{G}_j+\mathbf{k})\cdot\mathbf{r}} . \quad (16)$$

The matrix elements for the nonlocal potential [Eq. (9)] are

$$V_{\mathrm{nonlocal},l}(\mathbf{G}_j+\mathbf{k},\mathbf{G}_i+\mathbf{k})=\frac{2l+1}{4\pi\Omega}P_l(\cos\gamma)\times\int_0^\infty V_{\mathrm{nonlocal},l}(r)j_l(|\mathbf{G}_j+\mathbf{k}|r)\times j_l(|\mathbf{G}_i+\mathbf{k}|r)r^2dr , \quad (17)$$

where l is the angular-momentum quantum number, Ω is the cell volume, $V_{\text{nonlocal},l}(r)$ is the nonlocal potential, $j_l(|\mathbf{G}+\mathbf{k}|r)$ are the spherical Bessel functions, and $P_l(\cos\gamma)$ are the Legendre polynomials with

$$\cos\gamma=\frac{(\mathbf{G}_j+\mathbf{k})\cdot(\mathbf{G}_i+\mathbf{k})}{|\mathbf{G}_j+\mathbf{k}||\mathbf{G}_i+\mathbf{k}|} . \tag{18}$$

If a Kleinman and Bylander[14] separable pseudopotential is used [Eq. (10)] the matrix elements are

$$V^{\text{KB}}_{\text{nonlocal},l}(\mathbf{q},\mathbf{q}')=\frac{1}{\Omega\langle\Phi^{\text{PP},0}_l(r)|V_{\text{nonlocal},l}(r)|\Phi^{\text{PP},0}_l(r)\rangle}\left[\int_0^\infty\Phi^{\text{PP},0}_l(r)V_{\text{nonlocal},l}(r)j_l(|qr|)r^2\,dr\right]$$
$$\times\left[\int_0^\infty\Phi^{\text{PP},0}_l(r)V_{\text{nonlocal},l}(r)j_l(|q'r|)r^2\,dr\right]\sum_{m=-l}^{l}Y_{lm}(\hat{\mathbf{q}})Y^*_{lm}(\hat{\mathbf{q}}') , \tag{19}$$

where $Y_{lm}(\hat{\mathbf{q}})$ are the spherical harmonics.

In practice the expansion of Eq. (16) must be truncated at some point, and the wave function would only contain plane waves with a kinetic energy less than a chosen cutoff, $\frac{1}{2}(\mathbf{k}+\mathbf{G}_j)^2\le E_{\text{cut}}$. It is therefore desirable to reduce the high Fourier components of the crystal pseudo-wave-function by a suitable choice of a smooth pseudopotential, however there are certain natural limitations that occur. The atomic size imposes a length scale to the problem which determines how large any Fourier expansion of the pseudo-wave-function must be to accurately describe its properties. A smooth pseudopotential will avoid any unnecessarily large expansions, but cannot make the expansion arbitrarily short.

It has long been a matter of speculation about which atomic properties control the total-energy convergence in the solid. A very common misconception is that the Fourier transform of the pseudopotential $V(q)$ should decay rapidly to zero for large q. Although this is desirable, it is not of paramount importance. Rappe *et al.*[18] proposed recently that the decay of the Fourier transform of the atomic wave function $\Psi(q)$ provides a good estimation of the convergence rate in the solid. This is a good criterion, although, as we discuss later, it should be used with some caution. Looking at the local potential energy,

$$E^{\text{PP}}_{\text{local}}=\sum_j a(\mathbf{G}_j)\sum_i V_{\text{local}}(|\mathbf{G}_j-\mathbf{G}_i|)a(\mathbf{G}_i)$$
$$=\sum_i V_{\text{local}}(|\mathbf{G}_i|)\sum_j a(\mathbf{G}_j)a(\mathbf{G}_i-\mathbf{G}_j) , \tag{20}$$

we see that the local potential interacts in a complex fashion with the wave vector, mixing low-frequency components of the potential with high-frequency wave-vector components and *vice versa*. Examining the matrix elements that are neglected by the truncation of the Hamiltonian matrix [Eq. (15)], we find that a small number of large valued matrix elements corresponding to momentum transfers of $q\simeq 2\pi/d$, where d is a typical interatomic distance, are neglected. Also, a large number of small valued matrix elements corresponding to large momentum transfers are neglected. Finding a practical atomic criterion for pseudopotential smoothness is far from a trivial task, and the remaining portion of this section will present the results of our investigation into that problem.

In developing an improved nonlocal pseudopotential we started by generalizing the Kerker procedure[10] in such a way that we can generate a parametrized family of norm-conserving pseudopotentials. The first step is to continue the pseudo-wave-function inside the cutoff radius r_{cl} with an analytical function, which behaves as r^l for small r and has no nodes. With this in mind, Kerker defined the pseudo-wave-function as

$$R^{\text{PP}}_l(r)=\begin{cases}R^{\text{AE}}_l(r) & \text{if } r\ge r_{cl}\\ r^l\exp[p(r)] & \text{if } r\le r_{cl}\end{cases} , \tag{21}$$

where $p(r)$ is a polynomial of degree $n=4$,

$$p(r)=c_0+\sum_{i=2}^{n}c_i r^i . \tag{22}$$

In the polynomial expansion, the c_1 coefficient is not present to avoid a singularity of the screened pseudopotential $V_{\text{scr},l}(r)$ at $r=0$. The four coefficients of the polynomial are determined from the four conditions: (i) conservation of the charge enclosed within the core radius r_{cl} [Eq. (4)], and (ii)–(iv) the continuity of the pseudo-wave-function and its first two derivatives at r_{cl}. One then obtains the screened pseudopotential for $r<r_{cl}$ by inverting the radial Schrödinger equation [Eq. (6)], which can be explicitly written in this case as

$$V_{\text{scr},l}(r)=\begin{cases}V_{\text{AE}}(r) & \text{if } r\ge r_{cl}\\ \varepsilon_l+\dfrac{l+1}{r}\dfrac{p'(r)}{2}+\dfrac{p''(r)+[p'(r)]^2}{2} & \text{if } r\le r_{cl}\end{cases} . \tag{23}$$

A distinct advantage of this procedure is that the pseudo-wave-function $R^{\text{PP}}_l(r)$, and the screened pseudopotential $V_{\text{scr},l}(r)$, are analytic functions within the cutoff radius r_{cl}. We generalized[8] Kerker's method by simply increasing the order n of the polynomial $p(r)$; the additional coefficients give us the variational freedom needed for investigating smoothness properties for a parametrized family of pseudopotentials.

Smoothness can be easily achieved by increasing the cutoff radius r_{cl} at which the pseudopotential is generated. However, in the process of doing this the transferability of the pseudopotential is compromised. We would like to retain a constant transferability in order to justly determine if one pseudopotential is smoother than another. To do this, we used the logarithmic derivatives of the original Kerker pseudopotential as a reference for

TABLE I. The asymptotic dependencies (Ref. 19) for large q on the pseudopotential and pseudo-wave-function for the local pseudopotential, the nonlocal potential [Eq. (17)] for $l=0$, and the Kleinman and Bylander potential [Eq. (19)] for $l=0$. The $\Delta V^{(m)}$'s represent the difference between the derivatives of the local pseudopotential and the all-electron potential at the cutoff radii r_c and the function $P^{(m)}(0)$ represents derivatives of r times the pseudo-wave-function $rR(r)$ at the origin.

	Local	Nonlocal $l=0$	Kleinman and Bylander $l=0$
$1/q^3$	$\Delta V'(r_c)$	$V'_{\text{nonlocal}}(r_c)$	$V'_{\text{nonlocal}}(r_c)$
$1/q^4$	$\Delta V''(r_c)$	$V''_{\text{nonlocal}}(r_c)$	$V''_{\text{nonlocal}}(r_c)$
	$V'(0)$	$V'_{\text{nonlocal}}(0)$	$P'(0)V'_{\text{nonlocal}}(0)$
$1/q^5$	$\Delta V'''(r_c)$	$V'''_{\text{nonlocal}}(r_c)$	$V'''_{\text{nonlocal}}(r_c)$
$1/q^6$	$\Delta V^{(\text{IV})}(r_c)$	$V^{(\text{IV})}_{\text{nonlocal}}(r_c)$,	$V^{(\text{IV})}_{\text{nonlocal}}(r_c), P^{(\text{IV})}(0)V_{\text{nonlocal}}(0),$
	$V'''(0)$	$V'''_{\text{nonlocal}}(0)$	$P'''(0)V'_{\text{nonlocal}}(0), P'(0)V'''_{\text{nonlocal}}(0)$
$1/q^7$	$\Delta V^{(\text{V})}(r_c)$	$V^{(\text{V})}_{\text{nonlocal}}(r_c)$	$V^{(\text{V})}_{\text{nonlocal}}(r_c)$
$1/q^8$	$\Delta V^{(\text{VI})}(r_c)$	$V^{(\text{VI})}_{\text{nonlocal}}(r_c)$	$V^{(\text{VI})}_{\text{nonlocal}}(r_c), P^{(\text{VI})}(0)V_{\text{nonlocal}}(0), P^{(\text{V})}(0)V'_{\text{nonlocal}}(0),$
	$V^{(\text{V})}(0)$	$V^{(\text{V})}_{\text{nonlocal}}(0)$	$P^{(\text{IV})}(0)V''_{\text{nonlocal}}(0), P'''(0)V'''_{\text{nonlocal}}(0), P'(0)V^{(\text{V})}_{\text{nonlocal}}(0)$

transferability. The cutoff radii r_{cl} of our generalized pseudopotentials were then adjusted until their logarithmic energy derivatives matched the reference values. This procedure of determining the core radii will be used throughout the paper to assure a fair comparison between pseudopotentials.

We first studied the asymptotic behavior for large q. To do this we integrated by parts the Fourier transforms of the local pseudopotential and pseudo-wave-functions, the integrals for the nonlocal potential [Eq. (17)] for $|\mathbf{q}| \gg |\mathbf{q}'|$, and the q component of the separated Kleinman and Bylander potential [Eq. (19)]. In the first column of Table I we show how $V^{\text{PP}}_{\text{local}}(q)$ is dependent on the local potential $V^{\text{PP}}_{\text{local}}(r)$ for large q for up to $1/q^8$ behavior, where the ΔV^m represents

$$\Delta V^m(r) = \frac{d^m}{dr^m} V^{\text{AE}}(r) - \frac{d^m}{dr^m} V^{\text{PP}}_{\text{local}}(r) \ . \tag{24}$$

Similar results for the $l=0$ nonlocal and Kleinman and Bylander integrations are listed in columns 2 and 3, respectively, and are representative of the $l=\{1,2,3,\ldots\}$ cases. The dependencies for the pseudo-wave-function for $l=\{0,1,2,3\}$ are shown in Table II, where $P(r)=rR(r)$. As should be expected, the asymptotic behavior depends on the matching of derivatives at the cutoff radii. In Table I we can see a pattern, the asymptotic behavior the pseudopotential is dependent on the values of the odd derivatives of the pseudopotentials at the origin. The data in Table II reveals that the asymptotic behavior of the pseudo-wave-functions can be improved by setting all odd coefficients c_i to zero, which is the same as setting the old derivatives of the potentials at the origin to zero. We stress again that asymptotic behavior is helpful but not crucial in obtaining a smooth pseudopotential and, therefore, the information in Tables I and II should only be taken as a possible exploratory guide.

To test the above possibilities, we picked diamond and zinc blende as representative crystals containing first row and transition-metal elements, and proceeded to calculate the convergence of the total energy with respect to the basis set size for the different types of possible pseudopotentials. Setting the odd derivatives of the potentials at the origin to zero was easily accomplished. For the first derivative this translated into setting the c_3 coefficient to

TABLE II. The asymptotic dependencies (Ref. 19) for large q on the boundary conditions for the pseudo-wave-functions for the $l=\{0,1,2,3\}$ pseudo-wave-functions. The function $P^{(m)}$ represents derivatives of r times the pseudo-wave-function $rR(r)$, and the $\Delta P^{(i)}$'s represent the difference between the derivatives of the all-electron and pseudo-wave-functions at the cutoff radii r_c. For the derivatives at zero, the corresponding dependence on the c_i coefficients is also listed.

	$l=0$	$l=1$	$l=2$	$l=3$
$1/q^5$	$\Delta P'''(r_c)$	$\Delta P'''(r_c)$	$\Delta P'''(r_c)$	$\Delta P'''(r_c)$
$1/q^6$	$\Delta P^{(\text{IV})}(r_c)$, $P^{(\text{IV})}(0)\propto c_3\exp(c_0)$	$\Delta P^{(\text{IV})}(r_c)$	$\Delta P^{(\text{IV})}(r_c)$	$\Delta P^{(\text{IV})}(r_c)$
$1/q^7$	$\Delta P^{(\text{V})}(r_c)$	$\Delta P^{(\text{V})}(r_c)$ $P^{(\text{V})}(0)\propto c_3\exp(c_0)$	$\Delta P^{(\text{V})}(r_c)$	$\Delta P^{(\text{V})}(r_c)$
$1/q^8$	$\Delta P^{(\text{VI})}(r_c)$, $P^{\text{VI}}(0)\propto [c_2c_3+c_5]\exp(c_0)$	$\Delta P^{(\text{VI})}(r_c)$	$\Delta P^{(\text{VI})}(r_c)$ $P^{(\text{VI})}(0)\propto c_3\exp(c_0)$	$\Delta P^{(\text{VI})}(r_c)$

zero, and for the nth odd derivative the c_{n+2} coefficient is set to zero. Determining how many derivatives of the potential should be continuous at the cutoff radii involved balancing between improving the transferability of the pseudopotential and making the pseudopotential smoother. We found that the best results were obtained when two derivatives at the cutoff radii matched and all odd coefficients of c_n were set to zero, making the polynomial [Eq. (22)] of degree $n=10$.

To complete the generation procedure, we searched for a smoothness estimator that could be used to further improve the convergence rate for pseudopotentials with additional variational degrees of freedom. We tried using the minimization of the integral

$$\int_0^\infty |V_{\mathrm{scr},l}(q)| q^n dq \ , \tag{25}$$

to reduce the overall strength of the pseudopotential. We found that using $n=2$ produces a smooth pseudopotential. In a few cases the resulting pseudopotential was not optimal and therefore Eq. (25) should only be considered as a useful rule of thumb.

We also tested the minimization of the kinetic energy with reciprocal space wave vector $q > q_c$,

$$\int_{q_c}^\infty |\Psi(q)|^2 q^4 dq \leq \delta E_k \ , \tag{26}$$

as proposed by Rappe *et al.*[18] Their idea is that convergence is controlled by the kinetic energy of the atomic pseudo-wave-functions. We found that the generated pseudopotentials are extremely sensitive on the choice of q_c and this cutoff should be chosen using a procedure of the type suggesting by Rappe *et al.*. While the potentials generated with Eq. (26) show a fast total-energy convergence in the solid around $E_{\mathrm{cut}}=(1/2)q_c^2$, they produce pseudopotentials with strong short-wavelength oscillations. Comparison of pseudopotential and all-electron calculations for crystals indicated that these pseudopotentials may have transferability problems to the solid, which are not apparent from their atomic logarithmic derivatives.

Both Eqs. (25) and (26) can be used to optimize pseudopotentials that depend on several free parameters. We noticed that Eq. (25) produced pseudopotentials that are very flat near the origin, we therefore tested the condition

$$V''_{\mathrm{scr},l}(0)=0 \ , \tag{27}$$

as a smoothness controller for the case where the pseudopotential has only one free parameter. Because of its simplicity and effectiveness, this is the criterion for smoothness we prefer and use in the recipe of Sec. IV. This condition is actually quite reasonable, for if a pseudopotential is obviously too deep it has a positive second derivative at the origin, while if it is too shallow it has a negative second derivative at the origin. Therefore by enforcing the additional condition of zero curvature of the pseudopotential at the origin $V''_{l,\mathrm{scr}}(0)=0$, we are in fact selecting a value of $V_{l,\mathrm{scr}}(0)$ that is about right. This reasoning is illustrated in Fig. 1 using the carbon p pseudopotential, where we generated three p pseudopotentials, one with a positive curvature, one with a negative, and one with zero curvature at the origin. The s pseudopotential remained constant for all cases. It is clear from Fig. 1(b) that the pseudopotential satisfying Eq. (27) is not necessarily the one that has the fastest convergence for a given cutoff energy, but is rather the one with the best global convergence properties. For example, the potential with negative curvature at the origin has the fastest convergence at 36 Ry but then displays a poor convergence for cutoff energies between 40 and 80 Ry. Convergence could be optimized for a given cutoff energy or for a tolerated error in the relative total energy as suggested by Rappe *et al.*, however the gains of such a procedure are small and would yield a pseudopotential that would be far from optimal when used with another cutoff energy of tolerated error. The most important characteristic of the pseudopotentials obeying Eq. (27) is that they are very close to optimal for the entire range of cutoff energies.

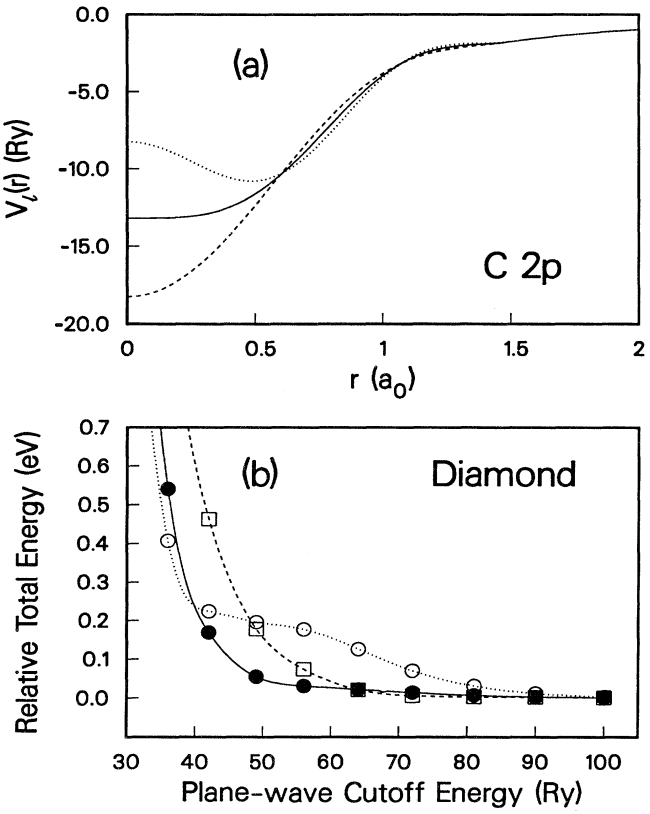

FIG. 1. The top panel (a) shows three examples of a screened p pseudopotential for carbon picked from a one parameter family of pseudopotentials. The bottom panel (b) shows the corresponding convergence of the calculated total energy of diamond per primitive cell with increasing plane-wave cutoff energy. The pseudopotential with zero curvature at the origin (solid line in both figures) has a better overall convergence than the pseudopotential with negative curvature (dotted line) or with positive curvature (dash line). In the bottom panel the circles and squares indicate the calculated values and the lines are obtained by a spline interpolation. The total energy is relative to the values calculated at 144 Ry.

IV. SIMPLE RECIPE FOR SMOOTH PSEUDOPOTENTIALS

In this section we present our favorite recipe for generating smooth pseudopotentials. The radial part of the pseudo-wave-function is first defined by Eq. (21), where $p(r)$ is a polynomial of order six in r^2,

$$p(r)=c_0+c_2r^2+c_4r^4+c_6r^6+c_8r^8+c_{10}r^{10}+c_{12}r^{12} . \tag{28}$$

The seven coefficients of the polynomial are determined from the following seven conditions, which we write down explicitly.

(i) Norm-conservation of charge within the core radius r_{cl},

$$2c_0+\ln\left[\int_0^{r_{cl}} r^{2(l+1)}\exp[2p(r)-2c_0]dr\right] =\ln\left[\int_0^{r_{cl}}|R_l^{\rm AE}(r)|^2r^2dr\right] . \tag{29a}$$

(ii)–(vi) The continuity of the pseudo-wave-function and its first four derivatives at r_{cl}, which in effect imposes the continuity of $V_{{\rm scr},l}(r)$ and its first two derivatives at r_{cl},

$$p(r_{cl})=\ln\left[\frac{P(r_{cl})}{r_{cl}^{l+1}}\right] , \tag{29b}$$

$$p'(r_{cl})=\frac{P'(r_{cl})}{P(r_{cl})}-\frac{l+1}{r_{cl}} , \tag{29c}$$

$$p''(r_{cl})=2V_{\rm AE}(r_{cl})-2\varepsilon_l -\frac{2(l+1)}{r_{cl}}p'(r_{cl})-[p'(r_{cl})]^2 , \tag{29d}$$

$$p'''(r_{cl})=2V'_{\rm AE}(r_{cl})+\frac{2(l+1)}{r_{cl}^2}p'(r_{cl}) -\frac{2(l+1)}{r_{cl}}p''(r_{cl})-2p'(r_{cl})p''(r_{cl}) , \tag{29e}$$

$$p''''(r_{cl})=2V''_{\rm AE}(r_{cl})-\frac{4(l+1)}{r_{cl}^3}p'(r_{cl}) +\frac{4(l+1)}{r_{cl}^2}p''(r_{cl})-\frac{2(l+1)}{r_{cl}}p'''(r_{cl}) -2[p''(r_{cl})]^2-2p'(r_{cl})p'''(r_{cl}) , \tag{29f}$$

where $P(r)=rR_l^{\rm AE}(r)$, $V_{\rm AE}(r)$ is the all-electron atomic screened potential, and the primes denote differentiation with respect to r.

(vii) The zero curvature of the screened pseudopotential at the origin $V''_{{\rm scl},l}(0)=0$ is as follows:

$$c_2^2+c_4(2l+5)=0 , \tag{29g}$$

which gives nicely smooth pseudopotentials.

The derivatives of the wave function and screened potentials are evaluated from the numerical all-electron wave function and screened potential using the seventh-order finite difference and the integration for the norm-conservation condition is also evaluated numerically. With the exceptions of Eqs. (29a) and (29g) all the equations are linear in c_i and are trivially solved with the Gauss-Jordan elimination. The nonlinear equations (29a) and (29g) are solved with the robust methods of false position and bisection, respectively. In the final step the screened pseudopotential is obtained through the standard method of inverting the Schrödinger equation [Eq. (6)], which in this case can be written explicitly [Eq. (23)].

V. PSEUDOPOTENTIAL COMPARISONS AND EXAMPLES

Using the procedure outlined in the preceding section, we generated both relativistic and nonrelativistic pseudopotentials for all elements with $Z<72$ and a few for $Z>72$. For all reasonable choices of the cutoff radii r_{cl}, a solution of the nonlinear equations [Eq. (29)] was readily obtained, showing the procedure to be stable. We have only encountered problems when the choice of r_{cl} was too close to a node of the all-electron wave function, in which case the norm-conservation [Eq. (4)] condition imposes a double hump shape in the radial pseudo-wave-function. We also found that as a result of equating both the first and second derivatives of the potential, the cutoff radii for our method can be chosen to be larger than those of other methods.[9–13] If we match pseudopotential transferability as outlined in the preceding section, we find that equivalent Kerker radii are $\approx(0.05-0.25)a_0$ smaller, and the Hamann-Schlüter-Chiang (HSC), Backelet-Hamann-Schlüter (BHS), and Vanderbilt radii are about half that of the present method.

We tested the convergence rate of the total energy of solids using the pseudopotentials of the procedure described in Sec. IV and compared them with those generated from other pseudopotential methods. We also checked that the pseudopotential calculations reproduce all-electron results for solids. We first compared the convergence rates for crystals containing first-row elements, namely carbon in the diamond structure and the two oxygen-containing materials rutile (TiO_2) and α-quartz-(SiO_2). Because these first-row elements contain no core p electrons, their p pseudopotentials are very strong, therefore materials containing these elements provide a stringent test for pseudopotential smoothness. For similar reasons we looked at copper, zinc sulfide, and rutile (TiO_2), which contain problematic d-electron transition metals. The two elements Cu and Zn represent the most difficult transition metals to use with plane waves, a result due to the extreme depth of the d pseudopotential and the localization of the d wave function. Last, we shall present results for cerium, a $4f$ rare-earth element.

We compared the convergence of the carbon pseudopotential with the pseudopotentials of Hamann, Schlüter, and Chiang,[9] Kerker,[10] and Vanderbilt.[13] We neglected the nonlocality for the $3d$ scattering channel and generated the pseudopotential in the non-spin-polarized groundstare valence configuration $2s^22p^2$. The cutoff radii are $r_{cs}=0.86a_0$ and $r_{cp}=0.82a_0$ for the HSC, $r_{cs}=1.43a_0$ and $r_{cp}=1.47a_0$ for the Kerker, $r_{cs}=r_{cp}=0.80a_0$ for the Vanderbilt, and $r_{cs}=1.50a_0$ and $r_{cp}=1.54a_0$ for the present method and correspond to pseudopotentials that

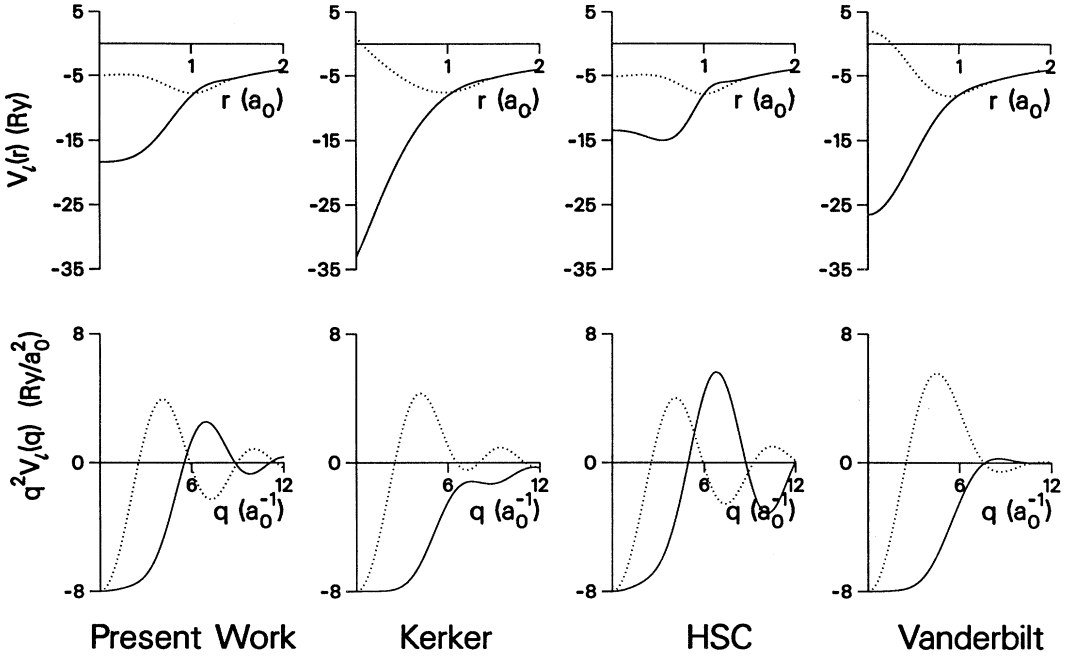

FIG. 2. The ionic pseudopotentials for carbon generated with the four different schemes are shown in both real and Fourier space. The dotted and solid curves correspond to the s and p pseudopotentials, respectively.

have the same logarithmic derivatives. These pseudopotentials and their Fourier transforms are compared in Fig. 2. The p pseudopotential of carbon is very deep and is the main factor controlling the total-energy convergence. A total-energy versus plane-wave cutoff energy E_{cut} curve for these pseudopotentials is shown in Fig. 3, with the total energies referenced to the total energy obtained at $E_{\text{cut}}=100$ Ry. The calculations were done with carbon in the diamond structure at the experimental lattice constant,[20] using two special **k** points and the semilocal form of the pseudopotential [Eq. (17)]. From the Fourier transforms, we can see that while the Vanderbilt transform decays much faster to zero than the present method it has a much slower convergence rate, confirming that a faster decay rate of the Fourier transform is not indicative of a fast total-energy convergence rate. An extremely shallow pseudopotential depth is also not a good convergence indicator, the HSC p pseudopotential is 5 Ry less deep than the current method, yet it has a slower convergence. For a total-energy convergence error less than 100 meV, the Vanderbilt and Kerker pseudopotentials require a matrix size of ~ 700, while the HSC pseudopotential requires a matrix size of ~ 1000 as compared with the present pseudopotential matrix size of ~ 450. From Fig. 3 we see that the total energy is converged to within 100 meV at a cutoff energy of $E_{\text{cut}}=49$ Ry with the present pseudopotential. The Kerker and Vanderbilt pseudopotentials show a smooth uniform convergence, while the HSC has a shoulder in the convergence at ~ 50 Ry, and the present method has a barely visible shoulder at ~ 60 Ry. This feature is quite important because if the total-energy convergence calculation had been stopped at 50 Ry, the HSC pseudopotential would apparently have had the fastest convergence.

Using the present pseudopotential we calculated the structural properties of diamond, using ten special **k** points in the irreducible wedge of the Brillouin zone, an energy cutoff of 49 Ry, and the Ceperley and Adler[21]

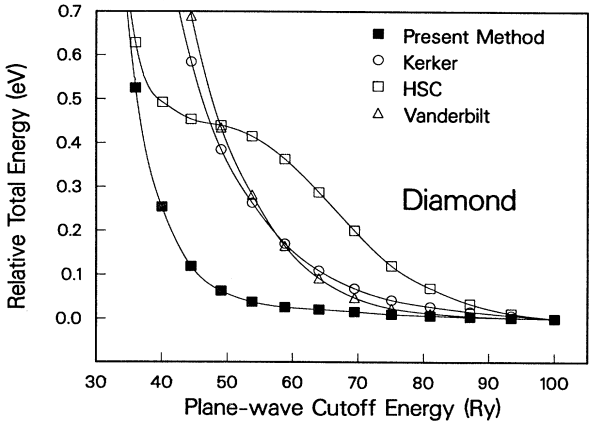

FIG. 3. The calculated total energy of diamond per primitive cell vs the cutoff energy of the plane-wave basis set for the four different pseudopotentials shown in Fig. 2. For each curve, the total energy is referenced to the total energy calculated for a cutoff energy of 100 Ry. The squares, circles, and triangles are the calculated data points and the curves are obtained by a spline interpolation.

TABLE III. We show structural and cohesive properties of diamond from pseudopotential plane wave (PP-PW), pseudopotential Gaussian-type orbital (PP-GTO), and LMTO calculations. The calculated values of the lattice constant a_0, bulk modulus B_0, pressure derivative of the bulk modulus B_0', and the cohesive energy E_c are compared with experiment.

	PP-PW[a]	PP-PW[b]	PP-GTO[c]	LMTO[d]	This work[e]	Expt.
a_0 (Å)	3.607	3.516	3.548	3.59	3.541	3.567[f]
B_0 (GPa)	517	503	444	430	455	443[g]
B_0'	2.52	3.99	3.24		3.77	4.0[h]
E_c (eV/atom)		8.34	8.17	8.2	8.80	7.37[i]

[a] Reference 24, using the Wigner exchange-correlation (xc) (Ref. 25), a BHS pseudopotential (Ref. 12), and a plane-wave cutoff energy of $E_{\text{cut}}=41$ Ry.
[b] Reference 26, using the Ceperley-Alder xc (Ref. 21), as parametrized by Perdew and Zunger (Ref. 22), a Kerker pseudopotential (Ref. 10), 10 **k** points, and $E_{\text{cut}}=50$ Ry.
[c] Reference 27, using the Hedin and Lundqvist xc (Ref. 28), a BHS pseudopotential (Ref. 12), and 10 **k** points.
[d] Reference 29, using the von Barth-Hedin xc (Ref. 30).
[e] This work uses the Ceperley-Alder xc (Ref. 21), as parametrized by Perdew and Zunger (Ref. 22), 10 **k** points, and $E_{\text{cut}}=49$ Ry.
[f] Reference 20.
[g] Reference 31.
[h] Reference 32.
[i] Reference 33.

correlation as parametrized by Perdew and Zunger.[22] The properties derived from a Murnaghan equation-of-state[23] fit to the calculated data points are listed in Table III, along with other calculated and experimental values. The agreement with experiment is typical of local-density calculations: it is good for the bond lengths and bulk modulus but there is a noticeable overestimate of the binding energy.

The convergence of the total energy with plane-wave cutoff is expected to be independent of the crystal environment in which it is used. This is illustrated by Fig. 4 where we compare the total energy convergence of rutile-TiO_2 and α-quartz SiO_2, where in both cases, the deep p potential of oxygen controls the convergence. In Fig. 5 we show the oxygen pseudopotential and its Fourier transform. The pseudopotential was calculated in the $2s^2 2p^4$ non-spin-polarized valence configuration and the cutoff radii were $r_{cs}=r_{cp}=1.45a_0$. The nonlocal d component of the pseudopotential was neglected for the solid calculation and we used the nonlocal Kleinman and Bylander form [Eq. (19)] with the p pseudopotential as the local component. The total energies of both systems were then calculated as a function of plane-wave cutoff energy, using the experimental lattice parameters and internal coordinates,[34,35] and two special **k** points in the reduced Brillouin zone for the rutile structure and one special **k** point for the α-quartz structure. In Fig. 4, the total energy is given per molecular unit, and the convergence curves are referenced to the total energy calculated at $E_{\text{cut}}=144$ Ry. As the figure shows, the two different structures have nearly identical convergence curves, indicating that the oxygen pseudopotential convergence does not depend on the choice of oxide. The equivalent cutoff radii for a BHS oxygen pseudopotential with the same logarithmic derivatives is $\sim 0.73a_0$. This is slight smaller than the core radii recently suggested for a BHS oxygen pseudopotential.[36] The convergence curve for that pseudopotential would still be off scale of Fig. 4 at 60 Ry. The electronic and structural properties of the two oxides calculated with the present pseudopotential are in good agreement with experiment and will be published elsewhere.[37,38]

There has been several recent all-electron and pseudopotential calculations for copper,[39–42] making it an interesting test of the new pseudopotentials. We compared the total energy convergence characteristic of the present pseudopotential with the pseudopotentials generated us-

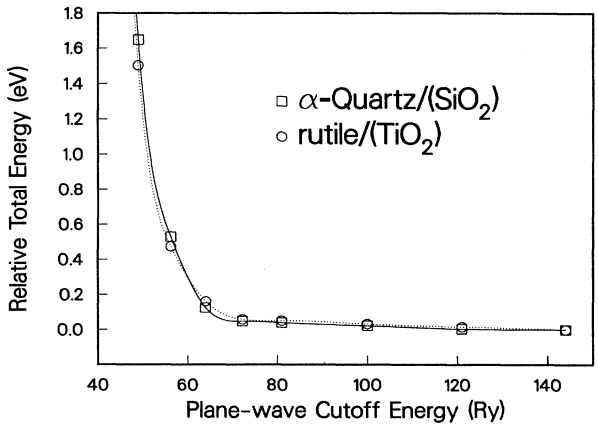

FIG. 4. The calculated total energy for α-quartz and rutile per molecular unit vs the cutoff energy of the plane-wave basis set. The total energies are referenced to the total energy obtained using a cutoff energy of 144 Ry. The squares and circles are the calculated data points and the solid and dotted curves are obtained from a spline interpolation.

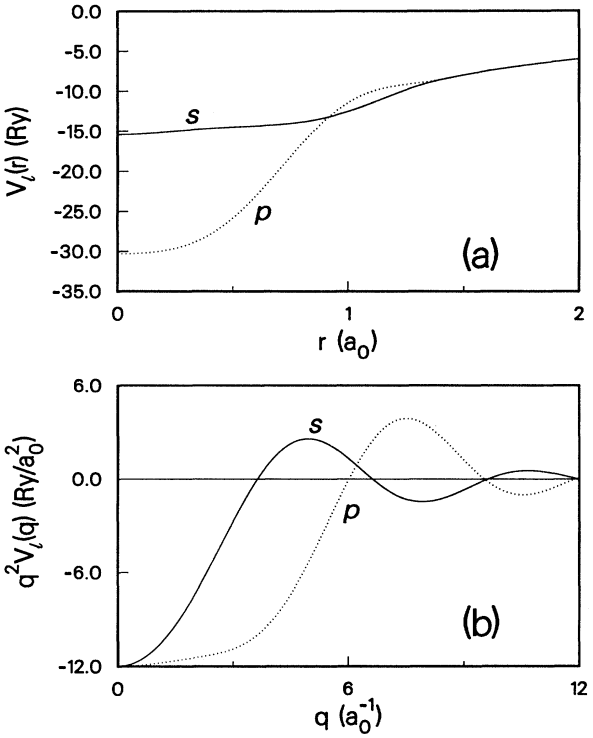

FIG. 5. The top panel (a) shows the ionic oxygen pseudopotential in real space generated using the present method and its Fourier space plot is shown in the bottom panel (b). The solid and dotted curves correspond to the s and p pseudopotentials, respectively.

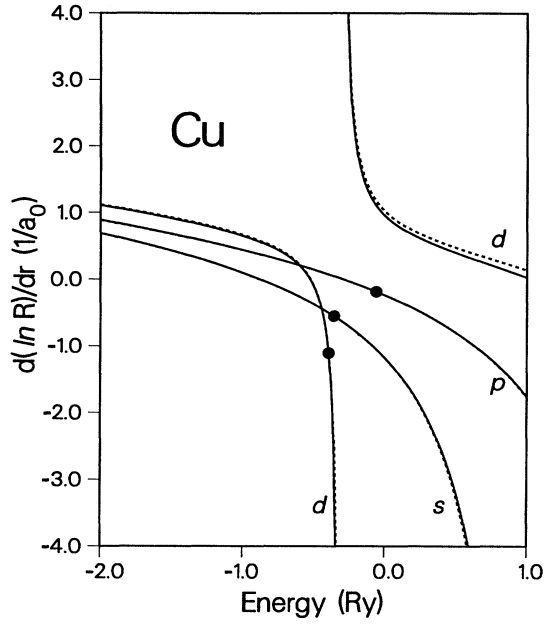

FIG. 6. The logarithmic derivatives [Eq. (11)] of the all-electron (solid line) and separated pseudopotential (dashed line) for the s, p, and d radial wave functions for atomic Cu are shown at a radius of $r_0 = 2.6a_0$. The atomic eigenvalues are indicated by the solid circles. The close agreement between the two sets of curves in an indication of the high transferability of the pseudopotentials. The absence of ghost states in the Kleinman and Bylander form of the pseudopotential is clearly shown.

ing the methods of HSC,[9] Vanderbilt,[13] and Kerker.[10] All four pseudopotentials were generated from a relativistic all-electron calculation of the copper valence ground state $3d^{10}4s^14p^0$, and then weighted averaged over the $j+\frac{1}{2}$ and $j-\frac{1}{2}$ orbitals.[43] As before, the cutoff radii were adjusted to provide a similar transferability as measured by the logarithmic derivative plots (Fig. 6). In Fig. 6 we have plotted the logarithmic derivatives calculated using the separated Kleinman and Bylander form of the pseudopotentials [Eq. (10)], demonstrating the absence of "ghost states"[16,44,45] in the plotted energy range. The equivalent cutoff radii are $r_{cs}=r_{cp}=1.10a_0$ and $r_{cd}=1.00a_0$ for the HSC, $r_{cs}=r_{cp}=1.20a_0$ and $r_{cd}=1.09a_0$ for the Vanderbilt, $r_{cs}=1.98a_0$ and $r_{cp}=r_{cd}=2.08a_0$ for the Kerker, and $r_{cs}=r_{cd}=2.08a_0$ and $r_{cp}=2.30a_0$ for the present pseudopotentials. The pseudopotentials and their Fourier transforms are shown in Fig. 7. From that figure we can see that the HSC d pseudopotential is the most shallow but contains some extra wiggles, the Kerker pseudopotential has the deepest d potential and the Vanderbilt has the fastest decay in reciprocal space. We then separated the pseudopotentials using the Kleinman and Bylander procedure using the s potential as the local component. For each of the above four pseudopotentials we then calculated a total-energy curve as a function of plane-wave cutoff energy $E_{\rm cut}$, using ten special **k** points in the reduced Brillouin zone and the experimental fcc lattice constant.[46] The results of these calculations are plotted in Fig. 8, using the total energy calculated at $E_{\rm cut}=225$ Ry as the baseline reference energy. We again find that our pseudopotential has the fastest convergence. To obtain a total-energy convergence within ~ 100 meV, the Vanderbilt pseudopotential would require a matrix size of ~ 1550, the HSC would require a matrix of ~ 1800, the Kerker requires a matrix of at least 3000, and the present method needs only a matrix of ~ 850.

Using the present pseudopotential, generated from both nonrelativistic and relativistic all-electron atomic calculations, we calculated the structural properties of Cu in both the fcc and bcc structures using a plane-wave cutoff energy of $E_{\rm cut}=72.25$ Ry, which corresponds to a total-energy convergence of within ~ 100 meV. The calculations were carried out using 64 and 44 special **k** points in the irreducible wedge of the Brillouin zone for fcc and bcc, respectively, and the Ceperley and Adler[21] correlation as parametrized by Perdew and Zunger.[22] The properties derived from a Murnaghan equation-of-state[23] fit to the calculated data points are listed in Table IV. The agreement between the present pseudopotential calculation to that of the linearized-augmented-plane-wave calculation (LAPW) is excellent, both of which show similar deviations from experiment. The agreement with the accurate LAPW results is important because it shows that the pseudopotential approximation is excel-

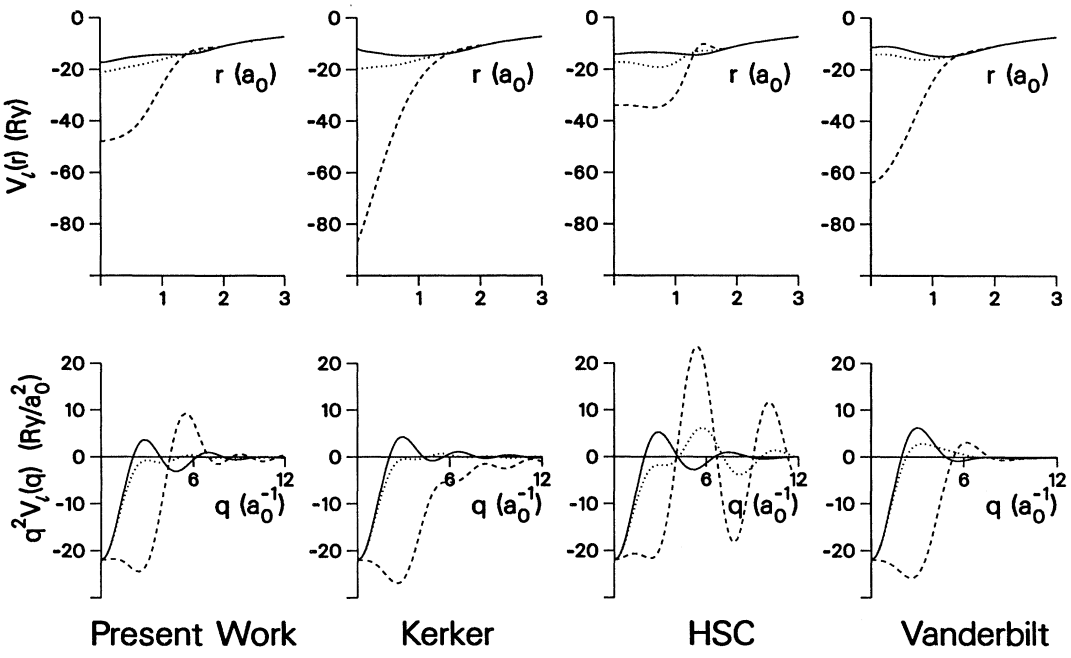

FIG. 7. The ionic copper pseudopotentials for four different pseudopotentials methods is shown in real space and Fourier space. The solid, dotted, and dashed curves correspond to the *s*, *p*, and *d* pseudopotentials, respectively.

lent (errors are smaller than LDA errors) and it demonstrates the transferability of our pseudopotentials. The 1.6% underestimated of the lattice constant and 0.85 eV overestimate of the binding energy compared with experimental values are typical of well-converged local-density calculations. Like the authors of Refs. 40 and 41, we did not find the double minimum for the bcc structure claimed by the authors of Ref. 39. The pseudopotential for Cu from Ref. 18 has a faster convergence rate of the total energy compared with ours, however the agreement with all-electron calculations is not as good as ours, suggesting a trade off between transferability to the solid and fast convergence of the plane-wave expansion.[49]

In a recent paper[50] we compared the results of an all-electron zinc-sulfide LAPW calculation to a pseudopotential calculation using the earlier version of our method described in Ref. 8. In that work we found excellent agreement between the pseudopotential and all-electron

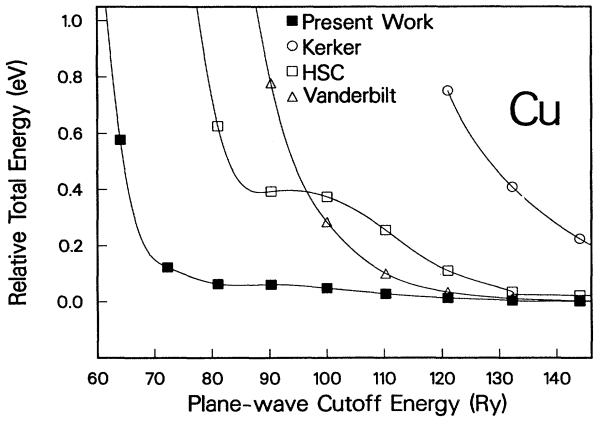

FIG. 8. The calculated total energy of fcc Cu plotted against the cutoff energy of the plane-wave basis set for the four pseudopotentials shown in Fig. 7. The total energy for all four curves are referenced to the total energy calculated at a cutoff energy of 225 Ry. The squares, circles, and triangles are the calculated data points and the curves are obtained from a spline interpolation.

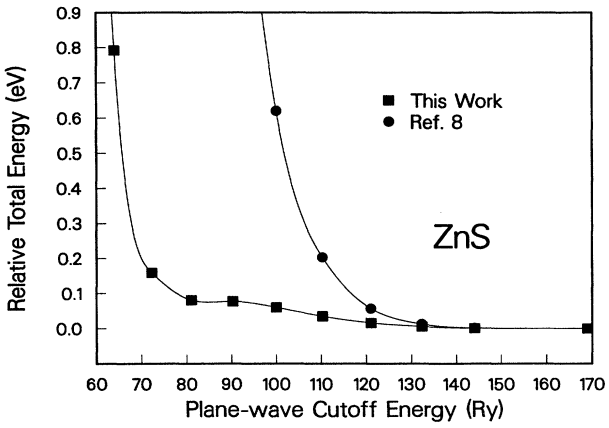

FIG. 9. The calculated total energy of ZnS plotted against the cutoff energy of the plane-wave basis set for pseudopotentials generated from the present method and the method of Ref. 8. The total energies are referenced to the total energy obtained with a cutoff energy of 169 Ry. The squares and circles are the calculated data points and the curves are obtained from a spline interpolation.

TABLE IV. We show structural and cohesive properties of fcc Cu and bcc Cu from pseudopotential mixed basis PP-MB, LAPW, PP-GTO, and PP-PW methods, for semirelativistic (SR) and nonrelativistic (NR) calculations. The calculated values of the lattice constant a_0, bulk modulus B_0, pressure derivative of the bulk modulus B_0', and the cohesive energy E_c are compared with experiment.

	PP-MB (SR)[a]	LAPW (SR)[b]	This work (SR)[c]	PP-GTO (NR)[d]	PP-PW (NR)[e]	LAPW (NR)[b]	This work (NR)[c]	Expt.
a_0 (fcc) (Å)	3.62	3.56	3.57	3.62	3.71	3.61	3.60	3.61[f]
a_0 (bcc) (Å)	2.81,2.93	2.84	2.84	2.87		2.86	2.86	
B_0 (fcc) (GPa)	150	183	174	188	148	162	160	142[g]
B_0 (bcc) (GPa)	126	179	175	185		160	160	
B_0' (fcc)			5.2				5.1	5.28[g]
B_0' (bcc)			5.3				5.1	
E_c (fcc) (eV)	3.35	4.42	4.38	3.83	3.90	4.14	4.19	3.50[h]
E_c (bcc) (eV)	3.31	4.37	4.35	3.81		4.12	4.16	
ΔE (meV)	41	49	25	20		18	22	

[a] Reference 39, using the Ceperley-Alder xc (Ref. 21), as parametrized by Perdew and Zunger (Ref. 22), a BHS pseudopotential (Ref. 12), and 29 (30) **k** points for fcc (bcc).
[b] Reference 40, using the Wigner xc (Ref. 25) and 60 (40) **k** points for fcc (bcc).
[c] This work uses the Ceperley-Alder xc (Ref. 21), as parametrized by Perdew and Zunger (Ref. 22), 60 (44) **k** points for fcc (bcc), and $E_{cut}=72.25$ Ry.
[d] Reference 41, using the Hedin and Lundqvist xc (Ref. 28), a Kerker pseudopotential (Ref. 10), and 60 (44) **k** points for fcc (bcc).
[e] Reference 18, using 44 **k** points and $E_{cut}=49$ Ry.
[f] Reference 46.
[g] Reference 47.
[h] Reference 48.

methods for both structural and electronic properties, demonstrating the high transferability of our pseudopotential generation procedure. The structural and electronic results calculated with the present pseudopotential are very similar to those of Ref. 50 and are in good agreement with accurate all-electron calculations. However, the energy convergence with the basis set size is faster with our present recipe (Fig. 9). The only significant difference between the present and old schemes is in the use of an even polynomial instead of a mixed polynomial in Eq. (22). Both calculations used the Kleinman and Bylander separation procedure on the pseudopotential and the experimental lattice constant.[51] In both cases the s potential was treated as the local component to avoid p and d ghosts states. A total-energy convergence of 100 meV is achieved with $\sim$3000 plane waves in the present method and $\sim$6000 plane waves in the earlier method.

The toughest job for a plane-wave expansion would be a $4f$ wave function. We have applied our method to Ce, and show in Fig. 10 the pseudopotential and its Fourier transform. The pseudopotential was generated using the valence configuration $6s^2 6p^0 5d^1 4f^1$ and the cutoff radii $r_{cs}=3.5a_0$, $r_{cp}=4.1a_0$, and $r_{cd}=r_{cf}=3.0a_0$. The corresponding total-energy curve for the experimental geometry[52] of α-Ce is shown in Fig. 11. The calculation was done using 10 special **k** points in the reduced Brillouin zone and the Ceperley-Adler[21] exchange correlation as parametrized by Perdew and Zunger.[22] A convergence of total energy to within 100 meV is obtained with $\sim$1350 plane waves. The Fermi level for this system lies within the $4f$ band and therefore the curve in Fig. 11 is representative of the convergence in energy for the $4f$ electrons.

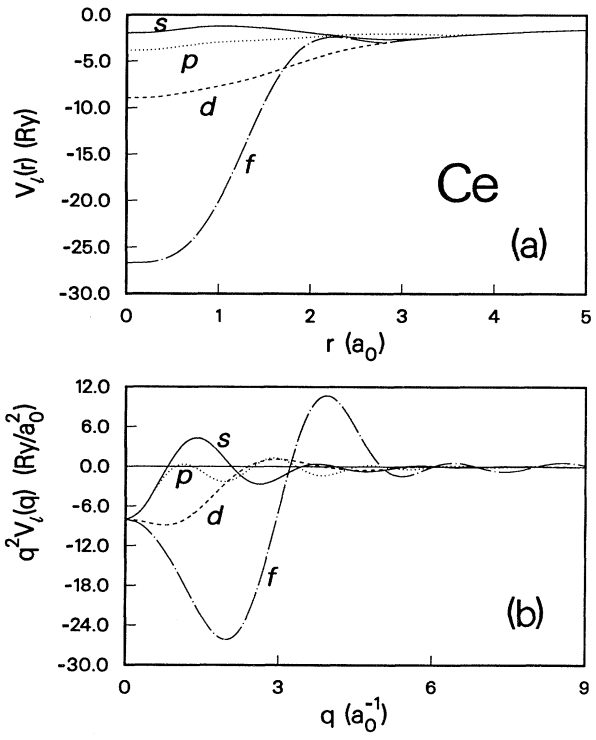

FIG. 10. The ionic cerium pseudopotential generated using the present method is shown in both real space, top panel (a) and Fourier space, bottom panel (b). The solid, dotted, dashed, and chain-dot curves correspond to the s, p, d, and f pseudopotentials, respectively.

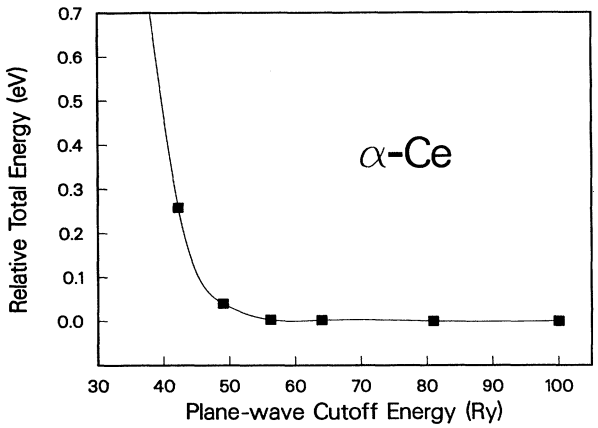

FIG. 11. The calculated total energy of α-Ce vs the cutoff energy of the plane-wave basis set. The total energies are referenced to the total energy obtained at a cutoff energy of 100 Ry. The squares are the calculated data points and the curve is obtained from a spline interpolation.

VI. CONCLUSIONS

We presented a simple recipe for generating smooth pseudopotentials for use in plane-wave calculations and illustrated their applicability with calculations of systems containing elements from several regions of the Periodic Table, including the transition metals and rare earths. To give an example of the improvements achieved, the benchmark pseudopotential from the BHS table for Zn would require a plane-wave cutoff energy of $\sim$900 Ry versus the $\sim$70 Ry of the present work. For zinc blende this means that $\sim$3000 plane waves can be used instead of $\sim$140 000. Of course, most of the improvement is due to the use of a larger core radius in our method. In our work we tried to make a fair comparison between different pseudopotentials by adjusting the core radii until their transferabilities, as judged by logarithmic derivative plots, were matched. The comparisons of Fig. 3 and Fig. 8 show that for these transferability matched pseudopotentials our method is better than other traditionally used pseudopotentials. Diagonalizing a matrix of 3000 by 3000 with a Givens-Householder algorithm would still be prohibitively expensive, as it would take 500 times longer to diagonalize than the 400 by 400 matrices of a LAPW calculation of equivalent precision. However, modern plane-wave codes using iterative diagonalization procedures can easily work with such matrices. In our case the fully self-consistent total energy for ZnS with the 3000 plane-wave matrices took only 2 min on a single Cray-2 processor, the 100 meV total-energy converged Ce and rutile calculation required 6 min ($\sim$1350 plane waves) and 4 min ($\sim$3800 plane waves), respectively. For α-quartz, determination of the minimum total energy with respect to the internal coordinates for a given lattice constant required $\sim$1 h ($\sim$6000 plane waves) on a single Cray-2 processor.

We have shown that, used with iterative diagonalization methods, our pseudopotentials can be used to study crystals containing elements from any region of the Periodic Table. The old restrictions limiting the pseudopotential plane-wave method to certain regions of the Periodic Table are obsolete, because these new pseudopotentials are as efficient and accurate as the best all-electron methods for first row atoms, transition metals, and rare earths.

ACKNOWLEDGMENTS

We are grateful to Professor J. R. Chelikowsky for stimulating discussions on the generation of pseudopotentials. We thank Dr. S.-H. Wei for providing us with high-quality all-electron calculations for comparison, and A. Rappe for providing a tabulation of the pseudopotentials of Ref. 18. This work was supported by a computer-time grant from the Minnesota Supercomputer Institute.

[1]P. Hohenberg and W. Kohn, Phys. Rev. **136**, B864 (1964); W. Kohn and L. J. Sham, *ibid.* **140**, A1133 (1965).

[2]E. Fermi, Nuovo Cimento **11**, 157 (1934).

[3]J. C. Phillips and L. Kleinman, Phys. Rev. **116**, 287 (1959).

[4]J. Ihm, A. Zunger, and M. L. Cohen, J. Phys. C **12**, 4409 (1979).

[5]For an excellent review see W. E. Pickett, Comput. Phys. Rep. **9**, 115 (1989).

[6]O. K. Andersen, Phys. Rev. B **12**, 3060 (1975); S.-H. Wei and H. Krakauer, Phys. Rev. Lett. **55**, 1200 (1985); C. T. Chang, D. Vanderbilt, S. G. Louie, and J. R. Chelikowsky, Phys. Rev. B **33**, 7941 (1986); P. Bendt and A. Zunger, *ibid.* **26**, 3114 (1982); O. K. Andersen and O. Jepsen, Phys. Rev. Lett. **53**, 2571 (1984); H. F. J. Jansen and A. J. Freeman, Phys. Rev. B **30**, 561 (1984).

[7]R. Car and M. Parrinello, Phys. Rev. Lett. **55**, 2471 (1985); J. L. Martins and M. L. Cohen, Phys. Rev. B **37**, 6134 (1988); M. C. Payne, J. D. Joannopoulos, D. C. Allan, M. P. Teter, and D. H. Vanderbilt, Phys. Rev. Lett. **56**, 2656 (1986); M. P. Teter, M. C. Payne, and D. C. Allan, Phys. Rev. B **40**, 12 255 (1989).

[8]N. Troullier and J. L. Martins, Solid State Commun. **74**, 613 (1990).

[9]D. R. Hamann, M. Schlüter, and C. Chiang, Phys. Rev. Lett. **43**, 1494 (1979).

[10]G. P. Kerker, J. Phys. C **13**, L189 (1980).

[11]A. Zunger and M. L. Cohen, Phys. Rev. B **18**, 5449 (1978).

[12]G. B. Bachelet, D. R. Hamann, and M. Schlüter, Phys. Rev. B **26**, 4199 (1982).

[13]D. Vanderbilt, Phys. Rev. B **32**, 8412 (1985).

[14]L. Kleinman and D. M. Bylander, Phys. Rev. Lett. **48**, 1425 (1982).

[15]See R. W. Shaw and W. A. Harrison, Phys. Rev. **163**, 604 (1967); W. C. Topp and J. J. Hopfield, Phys. Rev. B **7**, 1295

(1974).
[16]D. R. Hamann, Phys. Rev. B **40**, 2980 (1989).
[17]E. L. Shirley, D. C. Allan, R. M. Martin, and J. D. Joannopoulos, Phys. Rev. B **40**, 3652 (1989).
[18]A. Rappe, K. Rabe, E. Kaxiras, and J. D. Joannopoulos, Phys. Rev. B **41**, 1227 (1990).
[19]Only the lowest order in n of a $1/q^n$ dependence for the derivatives at the cutoff radii is shown, higher orders of $1/q^n$ for them may also exist.
[20]J. Donohue, in *The Structures of the Elements* (Krieger, Malabar, FL, 1982).
[21]D. M. Ceperley and B. J. Adler, Phys. Rev. Lett. **45**, 566 (1980).
[22]J. P. Perdew and A. Zunger, Phys. Rev. B **23**, 5048 (1981).
[23]F. D. Murnaghan, Proc. Nat. Acad. Sci. **30**, 244 (1944).
[24]P. E. Van Camp, V. E. Van Doren, and J. T. Devreese, Phys. Rev. B **38**, 12 675 (1988).
[25]E. Wigner, Phys. Rev. **46**, 1002 (1934).
[26]J. L. Martins and A. Zunger, Phys. Rev. Lett. **56**, 1400 (1986).
[27]S. Fahy and S. G. Louie, Phys. Rev. B **36**, 3373 (1987).
[28]L. Hedin and B. I. Lundqvist, J. Phys. C **4**, 2064 (1971).
[29]W. R. L. Lambrecht and O. K. Andersen, Phys. Rev. B **34**, 2439 (1986).
[30]U. von Barth and L. Hedin, J. Phys. C **5**, 1629 (1972).
[31]H. J. McSkimin and P. Andreatch, Jr., J. Appl. Phys. **43**, 985 (1972).
[32]K. Geschneider, Jr., in *Solid State Physics,* edited by F. Seitz, D. Turnbull, and H. Ehrenreich (Academic, New York, 1964), Vol. 16, p. 275.
[33]*Landolt-Börnstein Numerical Data and Functional Relationships in Science and Technology, New Series,* edited by O. Madelung (Springer, Berlin, 1982), Vol. 17a.
[34]S. C. Abrahams and J. L. Bernstein, J. Chem. Phys. **55**, 3206 (1971).
[35]W. G. Wyckoff, *Crystal Structures,* 4th ed. (Interscience, New York, 1974).
[36]Y. Bar-Yam, S. T. Pantelides, and J. D. Joannopoulos, Phys. Rev. B **39**, 3396 (1989).
[37]K. M. Glassford, N. Troullier, J. L. Martins, and J. R. Chelikowsky, Solid State Commun. **76**, 635 (1990).
[38]J. R. Chelikowsky, H. E. King, Jr., N. Troullier, J. L. Martins, and J. Glinneman, Phys. Rev. Lett. (to be published).
[39]M. H. Kang, R. C. Tater, E. J. Mele, and P. Soven, Phys. Rev. B **35**, 5457 (1987); I. A. Morrison, M. H. Kang, and E. J. Mele, Phys. Rev. B **39**, 1575 (1989).
[40]Z. W. Lu, S.-H. Wei, and A. Zunger, Phys. Rev. B **41**, 2699 (1990).
[41]J. R. Chelikowsky and M. Y. Chou, Phys. Rev. B **38**, 7966 (1988).
[42]K. Terakura, T. Oguchi, T. Mohri, and K. Watanabe, Phys. Rev. B **35**, 2169 (1987).
[43]L. Kleinman, Phys. Rev. B **21**, 2630 (1980); G. B. Bachelet and M. Schlüter, *ibid.* **25**, 2103 (1982).
[44]D. M. Bylander and L. Kleinman, Phys. Rev. B **41**, 907 (1990).
[45]X. Gonze, P. Käckell, and M. Scheffler, Phys. Rev. B **41**, 12 264 (1990).
[46]*American Institute of Physics Handbook,* 3rd ed. (McGraw-Hill, New York, 1972), Table 9d-3.
[47]P. van 't Klooster, N. J. Trappeniers, and S. N. Biswas, Physica B **97**, 65 (1979).
[48]R. Hultgren, R. L. Orr, and K. K. Kelly, in *Selected Values of Thermodynamic Properties of Metals and Alloys* (Wiley, New York, 1965).
[49]The authors of Ref. 18 informed us that the structural parameters quoted there may have some numerical noise unrelated to the pseudopotential.
[50]J. L. Martins, N. Troullier and S.-H. Wei, Phys. Rev. B (to be published).
[51]*Physics of II-VI and I-VII Compounds, Semimagnetic Semiconductors, Landolt-Börnstein New Series,* edited by K.-H. Hellwege (Springer-Verlag, Berlin, 1982), Group III, Pt. b.
[52]C. J. McHauge, H. C. Yakel, and L. K. Jetter, Acta Crystallogr. **10**, 832 (1957).